Optics Letters

Fast response of photorefraction in lithium niobate microresonators

Haowei Jiang,[1,2,3] Rui Luo,[2] Hanxiao Liang,[3] Xianfeng Chen,[1] Yuping Chen,[1,4] and Qiang Lin[2,3,5]

[1]State Key Laboratory of Advanced Optical Communication Systems and Networks, School of Physics and Astronomy, Shanghai Jiao Tong University, Shanghai 200240, China
[2]Institute of Optics, University of Rochester, Rochester, New York 14627, USA
[3]Department of Electrical and Computer Engineering, University of Rochester, Rochester, New York 14627, USA
[4]e-mail: ypchen@sjtu.edu.cn
[5]e-mail: qiang.lin@rochester.edu

Received 3 July 2017; revised 25 July 2017; accepted 25 July 2017; posted 26 July 2017 (Doc. ID 301416); published 17 August 2017

We present a detailed characterization of photorefraction in on-chip high-Q lithium niobate (LN) microresonators. We show that the photorefractive effect in these devices exhibits very distinctive temporal relaxation dynamics compared with those in bulk crystals and in mm-sized LN resonators. The relaxation of photorefraction is dominated by a fast time response with a time constant as small as 20.85 ms that is more than three-orders of magnitude faster than those observed in macroscopic devices. The observed fast response of photorefraction is of great potential as a convenient and energy-efficient approach for on-chip all-optical functionalities.

OCIS codes: (130.3730) Lithium niobate; (190.5330) Photorefractive optics; (140.3948) Microcavity devices.

https://doi.org/10.1364/OL.42.003267

Lithium niobate (LN), with rich optical properties [1], is probably one of the most widely studied and applied crystalline materials [2,3]. One unique characteristic is the photorefractive effect that arises from the photo-induced refractive index variation introduced by the combined photoconductive and electro-optic effects [4]. On the one hand, photorefraction functions as a promising approach for information storage [5,6]. On the other hand, photorefraction leads to optical damage of the LN crystal under high optical intensities, which becomes a major obstacle to the nonlinear photonic applications of LN [4,7]. In the past two decades, great efforts have been devoted to characterizing [8–14], understanding [4,15,16], and engineering [7,17–20] photorefraction. However, due to the small magnitude of photo-induced refractive index variation, accurate characterization of photorefraction turns out be a nontrivial task.

High-Q optical microresonators exhibit cavity resonances with narrow linewidths which are very sensitive to the refractive index variation of the device material. Indeed, this mechanism has been widely employed for sensing applications [21], which we have recently applied for ultrasensitive detection of the device temperature [22]. On the other hand, high-Q optical microresonators are able to dramatically enhance the optical field inside, which is convenient for exciting nonlinear optical processes [23]. Therefore, a high-Q LN microresonator would be an ideal device platform to study the photorefractive effect. This is particularly enabled by recent advances in LN microphotonics which result in high-Q LN microresonators available on a chip-scale platform [24–28].

In this Letter, we present a detailed characterization of photorefraction in on-chip high-Q LN microresonators. We show that photorefraction in on-chip LN devices exhibits rich time responses over a vastly different time scales over two–three orders of magnitude. In particular, we show that photorefraction in these devices exhibits intriguing fast time response in the order of approximately 10 ms that does not appear in bulk LN crystals or in mm-sized LN resonators [7–14,17–20]. This fast time response indicates that photorefraction in micro/nanophotonic LN devices is of great potential as a convenient and energy-efficient mechanism for all-optical functionalities, such as wavelength tuning and photonic circuit reconfiguration.

The device we employed is a high-Q LN microdisk resonator fabricated on a Z-cut congruent single-crystalline LN thin film on an insulator wafer (Fig. 1, inset), with a thickness of 400 nm and radius of 25 μm, sitting on a 2-μm high silica pedestal. The device was patterned through the electron-beam lithography and etched by an argon-ion milling process. More details of our device and fabrication processes can be found in our previous work [22,28]. The LN chip was placed on a thermoelectric cooler (TEC) with a fixed temperature set at 27°C. The TEC's temperature was stabilized by a temperature controller to prevent the temperature induced drifting of the device. The refractive index change induced by photorefraction excited by a laser launched into a cavity mode would be experienced by all other cavity modes in a similar fashion. Therefore, we employed a pump-probe scheme to sensitively characterize the resonance shift induced by photorefraction. Figure 1 shows the schematic of the experimental setup, where a strong pump laser is launched into a cavity resonance of the device to produce photorefraction, and a weak probe laser is launched into another cavity resonance to probe the induced resonance shift.

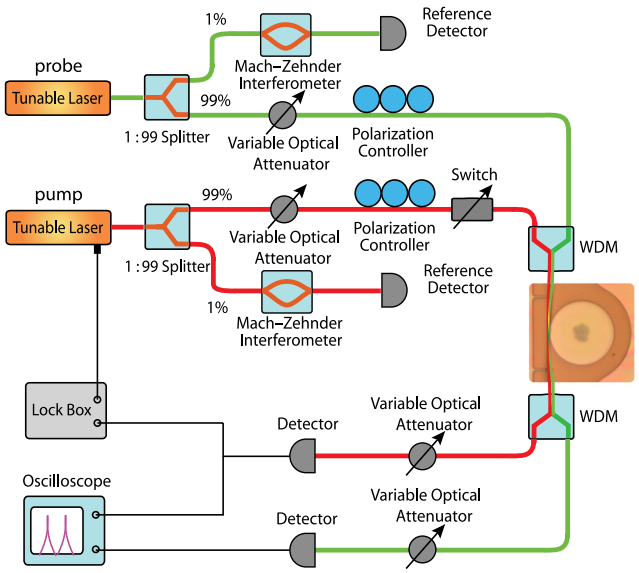

Fig. 1. Schematic of the experimental setup.

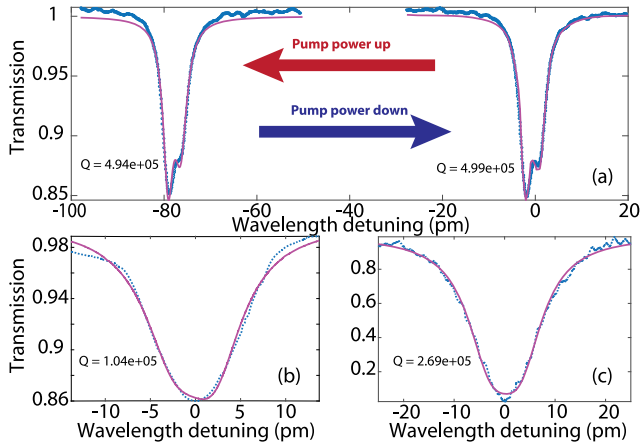

Fig. 2. Transmission spectra for the probe and pump modes, with experimental data shown in blue and theoretical fitting shown in red. (a) Transmission spectrum of the probe mode around 1528.4 nm. (b) and (c) Transmission spectra of the pump modes at 770.73 and 1548.78 nm, respectively.

We selected a high Q cavity mode at a telecom wavelength of approximately 1528.4 nm as the probe mode, which exhibits an optical Q of approximately 5×10^5 [Fig. 2(a)]. For the pump mode, we selected two cavity resonances at different wavebands to explore the wavelength-dependent behavior of photorefraction, one at 770.73 nm with a Q factor of 1.04×10^5 [Fig. 2(b)] which we designate as Pump Mode I, and the other at 1548.78 nm with a Q factor of 2.69×10^5 [Fig. 2(c)] which we designated as Pump Mode II. To quantify the photorefractive effect, the frequency of the pump laser is locked to one of these two resonances to introduce photorefraction, and the frequency of the probe laser is continuously scanned back and forth across the probe mode resonance to monitor the variation of its transmission spectrum. The power of the probe wave dropped into the cavity was maintained below 100 nW such that it introduces negligible nonlinear optical effect. The pump power is varied within a certain range that is significant enough to introduce a photorefractive effect but is small enough to prevent nonlinear optical oscillation [29].

To find the power dependence of the photorefractive effect, we recorded the transmission spectra of the probe mode at different pump powers. Figure 3 shows an example when the power of the Pump Mode II changes from 118 nW to 37.3 μW. It shows clearly that the probe resonance shifts towards blue with increased pump power, a typical feature of photorefraction. Mapping out the resonance wavelength as a function of the pump power, we obtained the red open circles in Fig. 4. Figure 4 compares the power dependence of probe resonance wavelength shift when pumping at two different wavebands. In both cases, the optical resonance shift induced by the photorefraction changes linearly with the pump power, as shown clearly in the insets of Fig. 4, which indicates a linear dependence of the induced refractive index change on the pump power. However, the magnitude of photorefraction induced by Pump Mode I at 770.73 nm is significantly larger than that induced by Pump Mode II at 1548.78 nm. This observation is consistent with other LN resonators [7,8,10], where the effect of photorefraction increases with decreased wavelength. For example, an optical power of 6.48 μW dropped into the Pump Mode I is able to shift the probe mode resonance by about 95 pm, corresponding to a refractive index change of 1.2×10^{-4} that is significantly larger than that induced by the thermo-optic effect or optical Kerr effect. Fitting the experimental data (Fig. 4, solid curves), we obtained a tuning rate of 14.6 pm/μW when pumping at Mode I, which is about 25 times greater than that when pumping at Mode II. The wavelength dependence may come from the multiphoton absorption coefficient increasing with the decreased wavelength [10,30]. Note that within these pump power ranges, the probe resonance shifts purely dispersively with the pump power, with negligible degradation of the optical Q, as shown in Fig. 3. This is seen more clearly in Fig. 2(a), where the transmission spectra of the probe mode at two different pump powers are nearly identical to each other except with an overall resonance shift.

To characterize the temporal relaxation of photorefraction in our device, we carried out ring-down measurement of the probe resonance. We first set the pump power at a certain constant level for a sufficiently long time until the probe mode becomes stable under the impact of photorefraction, and then abruptly switched off the pump power to zero and monitored

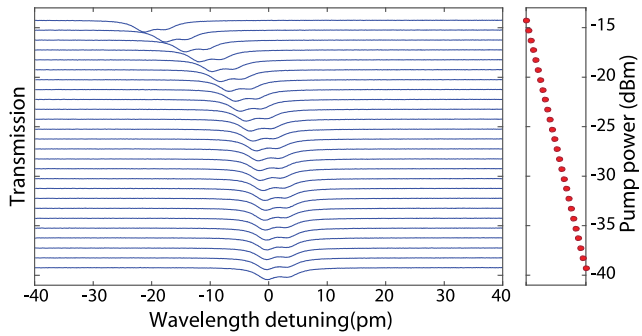

Fig. 3. Transmission spectra of the probe mode as a function of the power launched into the Pump Mode II at 1548.78 nm. The pump power for each trace is shown on the right.

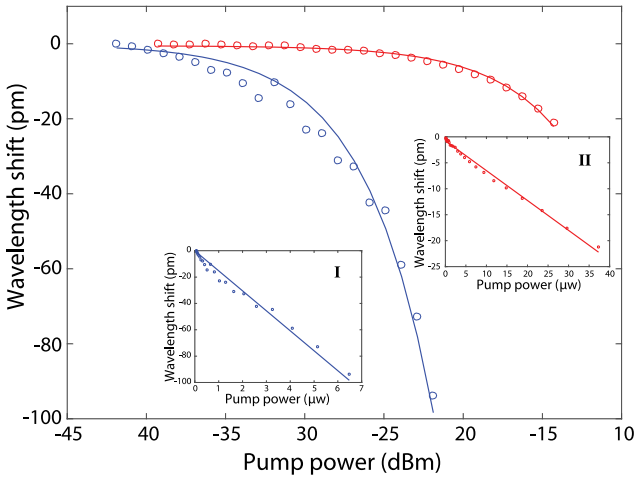

Fig. 4. Induced resonance shift of the probe mode as a function of the pump power. Blue and red show the cases for pump mode located at 770.73 and 1548.78 nm, respectively. The open circles show the recorded experimental data and the solid lines are linear fitting. Insets I and II plot the same curves but with pump power in the unit of μW, which shows clearly the linear power dependence.

the time dependent change of the transmission spectrum of the probe mode. Figure 5 shows an example of the ringdown of the probe resonance when pumping at Mode II. It shows that the probe resonance wavelength relaxes at a speed much faster than those observed in bulk LN crystals or in mm-sized LN resonators [7–14,17–20]. Mapping out the resonance wavelength shift as a function of time, we obtained the detailed time dependent relaxation of the probe resonance (Fig. 6). Figure 6 shows that the relaxation of photorefraction in the device exhibits rich temporal characteristics over different time scales. This is seen more clearly in the insets of Fig. 7 which plot the resonance shift in a logarithmic scale. The relaxation of photorefraction does not show a single exponential decay.

The complex time relaxation implies that there might exist multiple species of defect acceptors/donors that are involved in photorefraction [4], which exhibit distinctive time scales in trapping and releasing the created space charge carriers. Detailed analysis shows that the temporal relaxation of photorefraction-induced resonance shift of the probe mode can be well described by the following equation:

$$\delta\lambda = \alpha_1 e^{-t/\tau_1} + \alpha_2 e^{-t/\tau_2} + \alpha_3 e^{-t/\tau_3} + \alpha_4 e^{-t/\tau_4}. \quad (1)$$

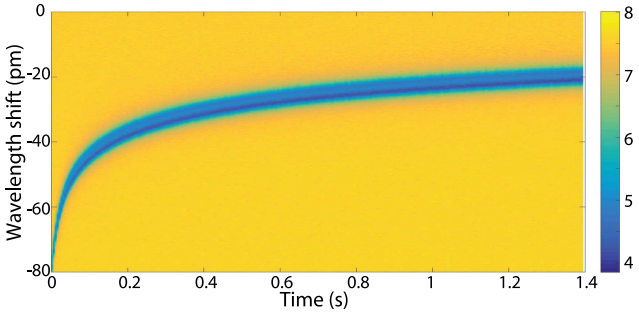

Fig. 5. Ring-down transmission spectra of the probe mode as a function of time after the pump power is switched off.

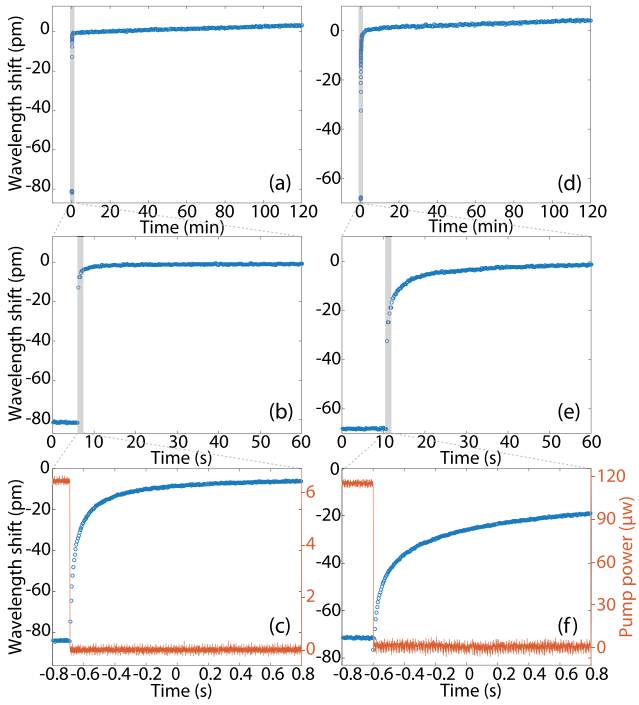

Fig. 6. Wavelength shift of the probe resonance as a function of time, after the pump power is switched off. (a)–(c) Ring-down of the probe resonance at different time scales, when pumping at Mode I at 770.73 nm. (d)–(f) Ring-down of the probe resonance at different time scales, when pumping at Mode II at 1548.78 nm. The red curves in (c) and (f) show the temporal waveform of the pump when its power is switched off. Before being switched off, the pump power dropped into the cavity is 6.48 and 117.7 μW, respectively, for Modes I (c) and II (f).

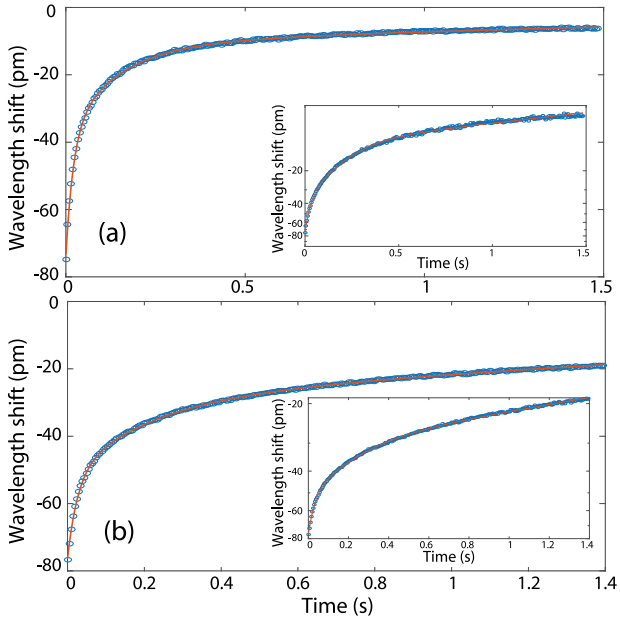

Fig. 7. Comparison of theoretical fitting with experimental data of photorefraction relaxation, with experimental data in blue and theoretical fitting in red. The pump wavelengths for (a) and (b) are 770.73 and 1548.78 nm. In the two figures, the insets plot the figures in a logarithmic scale.

Table 1. Fitted Parameters for the Relaxation of Photorefraction

λ_{pump}	α_1(pm)	α_2(pm)	α_3(pm)	α_4(pm)
770.73 nm	−34.956	−27.042	−10.153	−2.215
1548.78 nm	−23.535	−21.250	−24.314	−7.255
λ_{pump}	τ_1(ms)	τ_2(ms)	$\tau_3(s)$	$\tau_4(s)$
770.73 nm	20.85	137.8	2.127	6.757
1548.78 nm	25.67	187.7	1.959	28.44

By fitting the experimental data in Fig. 7 with Eq. (1), we obtained the time constants of photorefraction relaxation which are listed in Table 1. The relaxation of photorefraction exhibits rich temporal characteristics covering distinctive time scales over approximately three orders of magnitude. In particular, the relaxation of photorefraction in the device is dominated by a fast response with a time constant as small as 20.85 ms, which is more than three orders of magnitude faster than those observed in bulk LN crystals and in mm-sized LN resonators [7–14,17–20]. The fast response of photorefraction relaxation is likely due to the small physical size which dramatically limits the potential drift distance of created space charges. In particular, the small thickness of the device layer implies that the device surface might play an important role of charge recombination, which leads to fast relaxation of photorefraction.

Comparing the relaxation time constants induced by the Pump Modes I and II (Figs. 6 and 7), we can see that photorefraction introduced by Pump Mode II in the telecom band relaxes more slowly. This is likely because pumping at different wavelengths engages different species of defect acceptors/donors in the photorefractive process, which exhibits different time scales of trapping and releasing the created space charge carriers.

In conclusion, we have presented a detailed characterization of temporal relaxation of photorefraction in on-chip LN microresonators, by use of high-Q cavity resonance to excite and probe the photorefraction-induced refractive index variation. We showed that photorefraction in on-chip LN devices exhibits rich time responses with distinctive time scales over two–three orders of magnitude, which is particularly dominated by intriguing fast time response of approximately 20 ms that does not appear in bulk LN crystals or in mm-sized LN resonators [7–14,17–20]. Further exploration is required to understand the exact physical nature underlying such fast response. The observed fast time response indicates that photorefraction in micro/nanophotonic LN devices may open up a new avenue towards applications of on-chip all-optical functionalities.

Funding. National Natural Science Foundation of China (NSFC) (11574208, 61235009); National Science Foundation (NSF) (ECCS-1509749, ECCS-1610674); The Open Program of the State Key Laboratory of Advanced Optical Communication Systems and Networks at Shanghai Jiao Tong University (SJTU), China (2016GZKF0JT001); National Key R&D Program of China (2017YFA0303700).

Acknowledgment. This study was performed in part at the Cornell NanoScale Science and Technology Facility (CNF), a member of the National Nanotechnology Infrastructure Network.

REFERENCES

1. R. S. Weis and T. K. Gaylord, Appl. Phys. A **37**, 191 (1985).
2. L. Arizmendi, Phys. Status Solidi A **201**, 253 (2004).
3. M. Bazzan and M. Fontana, Appl. Phys. Rev. **2**, 040501 (2015).
4. P. Günter and J.-P. Huignard, eds., *Photorefractive Materials and Their Applications* (Springer, 2006).
5. J. F. Heanue, M. C. Bashaw, and L. Hesselink, Science **265**, 749 (1994).
6. K. Buse, A. Adibi, and D. Psaltis, Nature **393**, 665 (1998).
7. Y. Kong, S. Liu, and J. Xu, Materials **5**, 1954 (2012).
8. T. Fujiwara, S. Sato, and H. Mori, Appl. Phys. Lett. **54**, 975 (1989).
9. O. Beyer, I. Breunig, F. Kalkum, and K. Buse, Appl. Phys. Lett. **88**, 051120 (2006).
10. A. A. Savchenkov, A. B. Matsko, D. Strekalov, V. S. Ilchenko, and L. Maleki, Phys. Rev. B **74**, 245119 (2006).
11. P. Minzioni, I. Cristiani, V. Degiorgio, and E. P. Kokanyan, J. Appl. Phys. **101**, 116105 (2007).
12. S. M. Kostritskii, Appl. Phys. B **95**, 421 (2009).
13. G. Nava, P. Minzioni, I. Cristiani, N. Argiolas, M. Bazzan, M. V. Ciampolillo, G. Pozza, C. Sada, and V. Degiorgio, Appl. Phys. Lett. **103**, 031904 (2013).
14. M. Leidinger, C. S. Werner, W. Yoshiki, K. Buse, and I. Breunig, Opt. Lett. **41**, 5474 (2016).
15. M. Carrascosa, J. Villarroel, J. Carnicero, A. Garcia-Cabanes, and J. M. Cabrera, Opt. Express **16**, 115 (2008).
16. M. Kösters, B. Sturman, D. Haertle, and K. Buse, Opt. Lett. **34**, 1036 (2009).
17. K. Kitamura, Y. Furukawa, Y. Ji, M. Zgonik, C. Medrano, G. Montemezzani, and P. Günter, J. Appl. Phys. **82**, 1006 (1997).
18. Y. Kong, S. Liu, Y. Zhao, H. Liu, S. Chen, and J. Xu, Appl. Phys. Lett. **91**, 081908 (2007).
19. M. Kösters, B. Sturman, P. Werheit, D. Haertle, and K. Buse, Nat. Photonics **3**, 510 (2009).
20. D. Zheng, Y. Kong, S. Liu, M. Chen, S. Chen, L. Zhang, R. Rupp, and J. Xu, Sci. Rep. **6**, 20308 (2016).
21. M. R. Foreman, J. D. Swaim, and F. Vollmer, Adv. Opt. Photon. **7**, 168 (2015).
22. R. Luo, H. Jiang, H. Liang, Y. Chen, and Q. Lin, Opt. Lett. **42**, 1281 (2017).
23. K. J. Vahala, Nature **424**, 839 (2003).
24. T.-J. Wang, J.-Y. He, C.-A. Lee, and H. Niu, Opt. Express **20**, 28119 (2012).
25. C. Wang, M. J. Burek, Z. Lin, H. A. Atikian, V. Venkataraman, I.-C. Huang, P. Stark, and M. Lončar, Opt. Express **22**, 30924 (2014).
26. J. Lin, Y. Xu, Z. Fang, M. Wang, J. Song, N. Wang, L. Qiao, W. Fang, and Y. Cheng, Sci. Rep. **5**, 8072 (2015).
27. J. Wang, F. Bo, S. Wan, W. Li, F. Gao, J. Li, G. Zhang, and J. Xu, Opt. Express **23**, 23072 (2015).
28. W. C. Jiang and Q. Lin, Sci. Rep. **6**, 36920 (2016).
29. X. Sun, H. Liang, R. Luo, W. C. Jiang, X.-C. Zhang, and Q. Lin, Opt. Express **25**, 13504 (2017).
30. O. Beyer, D. Maxein, K. Buse, B. Sturman, H. T. Hsieh, and D. Psaltis, Phys. Rev. E **71**, 056603 (2005).